# The effect of reactions on the formation and readout of the gradient of Bicoid



2017 Phys. Biol. 14 016002

(http://iopscience.iop.org/1478-3975/14/1/016002)

IOP Publishing Phys. Biol. 14 (2017) 016002 doi:10.1088/1478-3975/aa56d9

Physical Biology

PAPER

# The effect of reactions on the formation and readout of the gradient of Bicoid

RECEIVED
11 August 2016

REVISED
22 December 2016

ACCEPTED FOR PUBLICATION
4 January 2017

PUBLISHED
8 February 2017

**Emiliano Perez Ipiña**[1,2,3] **and Silvina Ponce Dawson**[1]

[1] Departamento de Física, FCEN-UBA, and IFIBA, CONICET, Ciudad Universitaria, Pabellón I, (1428) Buenos Aires, Argentina
[2] Laboratoire J. A. Dieudonné Université de Nice Sophia Antipolis, UMR 7351 CNRS, Parc Valrose, F-06108 Nice Cedex 02, France
[3] Author to whom any correspondence should be addressed.

**E-mail:** emperipi@df.uba.ar

**Keywords:** Bicoid, SDD model, reactions, mathematical modelling, fluorescence

## Abstract

During early development, the establishment of gradients of transcriptional factors determines the patterning of cell fates. The case of Bicoid (Bcd) in *Drosophila melanogaster* embryos is well documented and studied. There are still controversies as to whether *SDD* models in which Bcd is *Synthesized* at one end, then *Diffuses* and is *Degraded* can explain the gradient formation within the timescale observed experimentally. The Bcd gradient is observed in embryos that express a Bicoid-eGFP fusion protein (Bcd-GFP) which cannot differentiate if Bcd is freely diffusing or bound to immobile sites. In this work we analyze an *SDID* model that includes the *Interaction* of Bcd with binding sites. We simulate numerically the resulting full reaction–diffusion system in a cylindrical domain using previously determined biophysical parameters and a simplified version of the Bcd source. In this way we obtain solutions that depend on the spatial location approximately as observed experimentally and that reach such dependence at a time that is also compatible with the experimental observations. Analyzing the differences between the free and bound Bcd distributions we observe that the latter spans over a longer lengthscale. We conclude that deriving the lengthscale from the distribution of Bcd-GFP can lead to an overestimation of the gradient lengthscale and of the Hill coefficient that relates the concentrations of Bcd and of the protein, Hunchback, whose production is regulated by Bcd.

## 1. Introduction

During the early development of embryos, cell differentiation is carried out by the transcriptional regulation of gene expression. The establishment of gradients of morphogens determines the patterns of cell fates. Cells get the information on their relative spatial location by 'reading' the local concentration of these morphogens (Wolpert 1969, Crick 1970). *Drosophila melanogaster* embryos constitute a model system in which this subject has been studied with great detail. In this system, bicoid (*bcd*), a maternal effect gene whose mRNA is localized at the anterior end of the embryo (St Johnston *et al* 1989, Little *et al* 2011), plays a key role. The protein, Bcd, one of the principal morphogenes in these embryos, is responsible, in conjunction with other factors, of the anterior–posterior (AP) axial patterning. *bcd* is translated into Bcd mainly at the anterior pole of the embryo (Little *et al* 2011), forming a concentration gradient along the anterior–posterior axis. Bcd is a transcription factor for over 20 target genes involved in the development. In particular, its role in the regulation of Hunchback is fundamental during the early embryogenesis of *Drosophila*. After fertilization, the cell undergoes several nuclear division cycles (n.c) without cytokinesis. After n.c. 7, nuclei move to the surface forming a syncytial blastoderm and ∼4 h after fertilization, just before cytokinesis begins (close to n.c. 14) there are approximately 6000 nuclei on the surface. Recently, live imaging using Bcd-GFP allowed the observation of the spatio-temporal distribution of Bcd during these early stages of the embryo development (Gregor *et al* 2007b). From these observations it was determined that the Bcd concentration gradient is established within the first 10 n.c., i.e. 90 min after egg deposition. Then, between n.c 10 and 14 the gradient remains almost unchanged and thereafter begins to decrease. The mechanisms by which the Bcd gradient is established so early are still not completely determined (Grimm *et al* 2010).

One of the simplest and most widely used models to explain the formation of the Bcd gradient is the *Synthesis*, *Diffusion*, *Degradation* (SDD) model (Driever and Nusslein-Volhard 1989, 1988, Struhl *et al* 1989). It assumes that Bcd is synthesized at a constant rate, $\zeta$, at the anterior end, then diffuses along the antero-posterior axis ($z$) of the embryo with diffusion coefficient, $D$, while it is being uniformly degraded with rate, $\alpha$. Assuming, for simplicity, a cylindrical embryo of transverse area, $A$, and total length, $L$, the dynamic equation of the Bcd concentration, [Bcd], in the SDD model can then be written as:

$$\frac{\partial\,[\mathrm{Bcd}]}{\partial t} = D\nabla^2[\mathrm{Bcd}] - \alpha[\mathrm{Bcd}], \tag{1}$$

with boundary conditions:

$$-D\frac{\partial\,[\mathrm{Bcd}]}{\partial z}A = \zeta, \quad z = 0$$
$$\frac{\partial\,[\mathrm{Bcd}]}{\partial z} = 0, \quad z = L. \tag{2}$$

For long enough $L$, in the region $z \gtrsim 0$, the solution of (1) and (2) is indistinguishable from the solution of:

$$\frac{\partial\,[\mathrm{Bcd}]}{\partial t} = D\nabla^2[\mathrm{Bcd}] - \alpha[\mathrm{Bcd}] + \frac{2\zeta}{A}\delta(z),$$
$$\frac{\partial\,[\mathrm{Bcd}]}{\partial z} = 0 \text{ for } z \to \pm\infty \tag{3}$$

where $\delta(z)$ is the Dirac delta function. The stationary solution of (3) is:

$$[\mathrm{Bcd}]\,(z) = [\mathrm{Bcd}]_o \exp(-z/z_o), \tag{4}$$

where $[\mathrm{Bcd}]_o = \zeta/(A\sqrt{\alpha D})$ and

$$z_o = \sqrt{D/\alpha}, \tag{5}$$

is the characteristic lengthscale of the gradient (Houchmandzadeh *et al* 2002). Observations of the Bcd distribution have led to the estimate $z_o \sim 100\ \mu$m. Within the framework of the SDD model, the time it takes for Bcd to diffuse over this distance is of the order of 100 $\mu$m$^2$/D. Thus, for the gradient to be established within 90 min it is necessary that $D \gtrsim 10^4\ \mu\mathrm{m}^2/(90\ \mathrm{min}) \sim 2\,\mu\mathrm{m}^2\,\mathrm{s}^{-1}$ (Gregor *et al* 2007b). The first quantification of the Bcd diffusion coefficient was obtained using Fluorescence Recovery After Photobleaching (FRAP) during mitosis (Gregor *et al* 2007b). The estimated value was $D_{\mathrm{FRAP}} \sim 0.3\ \mu\mathrm{m}^2\ \mathrm{s}^{-1}$ which was an order of magnitude too small to explain the establishment of the Bcd gradient within the SDD model during the experimentally observed times. In Bergmann *et al* (2007) it was argued that after nc 14 the gradient does not reach the steady state solution, so that (4) is not valid to estimate the diffusion rate. Other alternatives to the SDD model have also been proposed that involve active (Gregor *et al* 2007a), advective (Hecht *et al* 2009) or anomalous diffusive (Hornung *et al* 2005, Yuste *et al* 2010, Boon *et al* 2012) transport of Bcd. Another model stated that the stability of the gradient between n.c. 10 and 14 could be explained in terms of an underlying mRNA gradient (Spirov *et al* 2009). The distribution of mRNA was measured in Little *et al* (2011) finding that it is bell-shaped with an 80% concentrated within the 20% of the total embryo's length that lies closest to the anterior pole. This seems to discard the possibility that the Bcd gradient is a simple reflection of the way its mRNA is distributed along the axis. Regarding diffusion, the Bcd coefficient was measured again more recently using Fluorescence Correlation Spectroscopy (FCS) in the cytoplasm during interphase (Abu-Arish *et al* 2010) and in nuclei (Porcher *et al* 2010). The value estimated in the former was $D_{\mathrm{FCS}} \sim 7\ \mu\mathrm{m}^2\ \mathrm{s}^{-1}$ (Abu-Arish *et al* 2010). In that work the diffusion coefficient $D$ was also estimated using FRAP obtaining $D_{\mathrm{FRAP}} \sim 1\ \mu\mathrm{m}^2\ \mathrm{s}^{-1}$. Although the FCS result apparently reconciles the observed time it takes for the gradient to be formed with the SDD model, the question arises as to what is the reason for the discrepancy between $D_{\mathrm{FCS}}$ and $D_{\mathrm{FRAP}}$. In Sigaut *et al* (2014) an explanation was provided for this apparent discrepancy.

Based on previous studies on the transport of substances that diffuse and react (Pando *et al* 2006) and on the analysis of FCS and FRAP experiments in such a case (Sigaut *et al* 2010), it was shown in Sigaut *et al* (2014) that both the FRAP and FCS estimates of the Bcd diffusion coefficient (Gregor *et al* 2007b, Porcher *et al* 2010) could be correct if the interaction of Bcd with immobile or slowly moving binding sites was taken into account. Namely, if Bcd is assumed to diffuse with free coefficient, $D_f$, and react with binding sites, $S$, on more massive molecules according to:

$$\mathrm{Bcd} + S \underset{k_{\mathrm{off}}}{\overset{k_{\mathrm{on}}}{\leftrightarrows}} \mathrm{Bcd}_b, \tag{6}$$

its net transport can be described in terms of 'effective' diffusion coefficients. As shown in Pando *et al* (2006) the effective coefficient is different depending on whether one looks at the transport of a single molecule in which case it is:

$$D_{\mathrm{sm}} \equiv \frac{D_f + \frac{S}{K_d}D_S}{1 + \frac{S}{K_d}} \tag{7}$$

or at the dispersion of a collection of them in which case it is:

$$D_{\mathrm{coll}} \equiv \frac{D_f + \frac{[S]^2}{K_d[S_T]}D_S}{1 + \frac{[S]^2}{K_d[S_T]}}. \tag{8}$$

In (7) and (8), $D_S$ is the free diffusion coefficient of $S$ and of $\mathrm{Bcd}_b$, $K_d \equiv k_{\mathrm{off}}/k_{\mathrm{on}}$ is the dissociation constant of the reaction (6) and $[S]$ and $[S_T]$ are the free and the total binding site concentrations. FRAP provides an estimate of $D_{\mathrm{sm}}$ (Sprague and McNally 2005) and FCS gives estimates of $D_{\mathrm{sm}}$ and $D_{\mathrm{coll}}$ (Sigaut *et al* 2010). Interpreting the results of Gregor *et al* (2007b), Porcher *et al* (2010) within this framework the work of Sigaut *et al* (2014) showed that the FRAP and the FCS estimates of the Bcd diffusion coefficient were

compatible. Associating the estimated coefficients to $D_{sm}$ or $D_{coll}$, depending on the experiment, the concentrations and the dissociation constant were determined (Sigaut *et al* 2014). The aim of this previous work was to reconcile the apparently contradictory estimates of the Bcd diffusion coefficient derived with FRAP and FCS. Both FRAP and FCS are optical techniques in which the fluorescence coming from a relatively small region within the embryo is collected. Thus, it is possible to assume that all concentrations are uniform (and in equilibrium with one another) inside the observed region. This allows the analyses of the results to be performed with linear equations. In fact, this is what we did in Sigaut *et al* (2014) and, using the fast reaction approximation, we estimated free diffusion coefficients and the dissociation constant of the reaction, biophysical parameters that we expect should remain the same all along the antero-posterior axis of the embryo. In the current paper we use the fully nonlinear reaction–diffusion equations that describe the dynamics of Bcd and of binding sites that interact according to equation (6) with the parameters determined in Sigaut *et al* (2014) to study the spatio-temporal distribution of [Bcd] along the embryo. In this way we analyze the formation of the Bcd gradient within the context of a model that includes the *Interaction* of Bcd with binding sites together with its *Synthesis*, *Diffusion* and *Degradation*, i.e. within the context of an *SDID model*. It is most likely, however, that Bcd binds cooperatively to binding sites, not as prescribed by equation (6), and that it interacts with many different species, including DNA, mRNA, proteins and other cell components (Liu and Ma 1996, Rivera-Pomar *et al* 1996, Zhu and Hanes 2000, Guruharsha *et al* 2011). Furthermore, our simplified model does not distinguish between the cytoplasm and the interior of the nuclei. In this regard, it should be understood as some sort of 'effective' model in which the reaction scheme (6) represents all the processes that affect the net transport rate and free concentration of Bcd in the nucleus. Most of the sites that $S$ represents hinder the transport of Bcd. As determined by the analysis of Sigaut *et al* (2014) $S$ is either immobile or diffuses freely at a much slower rate ($D_S \sim 0.1\ \mu m^2\ s^{-1}$) than the free diffusion of Bcd ($D_f \sim 20\ \mu m^2\ s^{-1}$). The idea that the transport of Bcd is hindered by its interaction with a complex environment also underlies other approaches that describe this transport as sub-diffusive (Hornung *et al* 2005, Yuste *et al* 2010, Boon *et al* 2012). Here we take a different perspective in which the dynamics, while not being purely diffusive, takes into account all these complex interactions through the simplest possible reaction scheme (equation (6)). Our SDID model should then be interpreted as a toy model where to investigate how the characteristic length and time scales of [Bcd] are affected when the interaction with binding sites is considered. In spite of its simplicity, its predictions can be contrasted with the observations. Furthermore, it helps pinpoint the main drawbacks of interpreting the experimental observations without considering the effect of the interactions of Bcd. In particular, taking into account the distribution of Bcd-mRNA determined in Little *et al* (2011) we find that the SDID model can account for the formation of the bulk part of the Bcd gradient within the experimentally observed times. Although the formation of the gradient is a nonlinear process that involves several timescales, the analysis we present here confirms what was presumed in Sigaut *et al* (2014), i.e. that the *collective* effective coefficient, $D_{coll}$, gives a correct estimate of the order of magnitude of the time it takes for [Bcd] to converge to its corresponding stationary distribution.

An important aspect of the *bcd* morphogen system is the precise response of one of its main target genes, *hunchback* (*hb*). As well as *bcd*, *hb* is a maternal effect gene. In the early embryo, the *hb* mRNA is supplemented with zygotically transcribed mRNA which production is regulated by Bcd. The distribution of the resulting protein, Hb, presents very sharp borders along the AP axis, as an 'on/off' pattern. This indicates a high sensitivity of the *hb* mRNA to changes in the concentration of Bcd. This is consistent with a relationship between both concentrations with a high Hill coefficient that can be attributed to a cooperative binding of Bcd to some of the seven sites in the *hb* P2 enhancer that have been identified (Driever and Nusslein-Volhard 1989, Struhl *et al* 1989). In fact, in Gregor *et al* (2007a) it was proposed that both concentrations were related by:

$$\frac{[\mathrm{Hb}]}{[\mathrm{Hb}]_{max}} = \frac{[\mathrm{Bcd}]^n}{[\mathrm{Bcd}]^n + [\mathrm{Bcd}]_{1/2}^n}, \qquad (9)$$

with $n > 1$, the Hill coefficient, and $[\mathrm{Bcd}]_{1/2}$ the Bcd concentration at which [Hb] reaches half of its maximum value. Using embryos immunostained for DNA, Bcd and Hb, scatter plots of [Hb] versus [Bcd] were obtained in Gregor *et al* (2007a). From these plots a Hill coefficient, $n = 5$, was estimated. In spite of the relatively large value of $n$ and of the fluctuations that are intrisic to the transcription process (Little *et al* 2013), the scatter plots also showed a remarkable degree of precision between the distributions of Hb and Bcd (~10% near the point of half-maximal activation) (Gregor *et al* 2007a). The control experiments of Gregor *et al* (2007b) showed, on the other hand, that the fluorescence intensity obtained in antibody stainings was linearly related to the one collected from Bcd-GFP. The latter allows the observation of the spatio-temporal dynamics of [Bcd] *in vivo*. Further control experiments demonstrated that the GFP-tagging of Bcd did not alter its functionality, in particular, its ability to act as transcription factor. It is then likely that the GFP-tail does not affect the binding properties of Bcd to the various sites that are represented by $S$ in the scheme (6). Conversely, we may assume that the photophysical and photochemical properties of Bcd-GFP do not change with Bcd binding. It is under this assumption that the interpretation of the FCS and FRAP experiments that we presented in Sigaut *et al*

(2014) could explain various observations within a unified framework. In particular, if binding changed the fluorescence properties of Bcd, the auto-correlation function derived in FCS would not be characterized solely by diffusive timescales as obtained in Abu-Arish *et al* (2010) but would also have exponentially decaying terms (Sigaut *et al* 2016). The fact that the ACF of Abu-Arish *et al* (2010) is characterized by various diffusive timescales is an indication that the assumption that binding does not affect the fluorescence emission of Bcd-GFP is correct. This assumption implies that the fluorescence distribution observed in embryos that express Bcd-GFP comes from the total, rather than the free, Bcd concentration. This means that the actual dynamics of the free Bcd is hidden in the observations. As we show in the paper, considering the difference between the free Bcd and the observed fluorescence distributions can help explain the shift in the Hb on-off transition observed in Liu *et al* (2013) when the maximum Bcd concentration was different from that in wild type embryos. The difference between free Bcd and observed fluorescence also implies that the length and time scales of their distributions could differ as well. In fact, in the present paper we show that this is the case using the SDID model with realistic parameter values. Assuming that the lengthscale determined from the observations of Bcd-GFP corresponds to that of free Bcd can lead to incorrect estimations of the Bcd diffusion coefficient and/or degradation rate. The difference in the lengthscale of the free and the total [Bcd], on the other hand, can have implications for the relationship between [Bcd] and [Hb] that is derived from the fluorescence observations. As we show in the present paper the Hill coefficient that characterizes the relationship between the concentrations of Bcd and Hb can be different from the one that is directly derived from the scatter plot of the observed fluorescence. Although the Hill coefficient does not necessarily correspond to the degree of cooperativity with which Bcd binds to the sites on DNA that regulate the transcription of hb (see e.g. Estrada *et al* (2016)), it is an increasing function of the latter. Thus, re-interpreting the meaning of the Hill coefficient that characterizes the relation between the fluorescence profiles, as our theoretical studies indicate could be necessary, calls for a revision on the conclusions about the precision with which hb reads the [Bcd] distribution.

## 2. Methods

### 2.1. The SDID model

We consider a model in which Bcd is synthesized over a region of the anterior pole embracing 20% of the embryo, diffuses with free coefficient, $D_f$, interacts with a single type of binding sites according to (6) and is degraded at a constant rate. We consider a cylindrical domain in which all concentrations only vary along the axial coordinate, $z$, ($0 \leqslant z \leqslant L = 500\ \mu$m). We show a schematic representation of this domain in figure 1(a). The assumptions on the Bcd synthesis are based on the observations of Little *et al* (2011) according to which ~90% of the mRNA of Bcd is located in a region that starts at the anterior pole and extends up to 20% of the length of the embryo. Although the mRNA concentration in this anterior region is not perfectly uniform, we simplify its description and assume that *Bcd* is synthesized with a rate:

$$\theta(z) = \begin{cases} \theta_o & \text{if } z \leqslant 0.2L \\ 0 & \text{if } z > 0.2L \end{cases}, \tag{10}$$

where $\theta_o$ is constant. We assume that the binding sites are uniformly distributed over the whole embryo and, based on the analyses of Sigaut *et al* (2014), that they diffuse with coefficient, $D_S \ll D_f$. We thus assume that the binding sites belong to molecules that are either much more massive than Bcd or are attached to immobile cell components so that their mobility remains unaltered when they bind Bcd. In certain instances we also assume that they are immobile. We consider different alternative versions of the model that differ in the manner in which we treat Bcd degradation or in whether we include the dynamics of Bcd-GFP maturation or not. Cells have different systems to carry out the degradation of proteins and several regulatory mechanisms to ensure their selectivity. In many cases this involves the conjugation of ubiquitin to proteins to 'mark' them for their eventual degradation (see e.g. Lecker *et al* (2006)). Given that in our model $S$ represents a broad range of possible binding sites for Bcd, in principle it is not clear how the binding of Bcd to $S$ would affect the Bcd tagging process that precedes its degradation. It is for this reason that we consider two possibilities in this regard: one in which the rate of degradation is only proportional to the concentration of free Bcd and another one in which it is proportional to the concentration of total Bcd. Here we present the equations of the version that we call of 'partial degradation' because we assume that Bcd is degraded only in its free form. This version does not include the process of GFP maturation either. The equations of the other versions of the SDID model are described in the appendix. The spatio-temporal dynamics of the concentrations if Bcd is degraded only when free and the process of Bcd-GFP maturation is not included is given by:

$$\begin{aligned} \frac{\partial [\text{Bcd}]}{\partial t} &= D_f \nabla^2 [\text{Bcd}] - k_{\text{on}} [\text{Bcd}]([S_T] - [\text{Bcd}_b]) + k_{\text{off}} [\text{Bcd}_b] \\ &\quad - \tilde{\alpha} [\text{Bcd}] + \theta(z), \\ \frac{\partial [\text{Bcd}_b]}{\partial t} &= D_S \nabla^2 [\text{Bcd}_b] + k_{\text{on}} [\text{Bcd}]([S_T] - [\text{Bcd}_b]) - k_{\text{off}} [\text{Bcd}_b], \end{aligned} \tag{11}$$

where $[\text{Bcd}_T] = [\text{Bcd}] + [\text{Bcd}_b]$ and $[S_T] = [S] + [\text{Bcd}_b]$ are the total Bcd and binding site concentrations, respectively and $\tilde{\alpha}$ is the degradation rate. To simplify the notation we refer to the concentration of free Bcd as [Bcd]. It should not be confused with Bcd, which

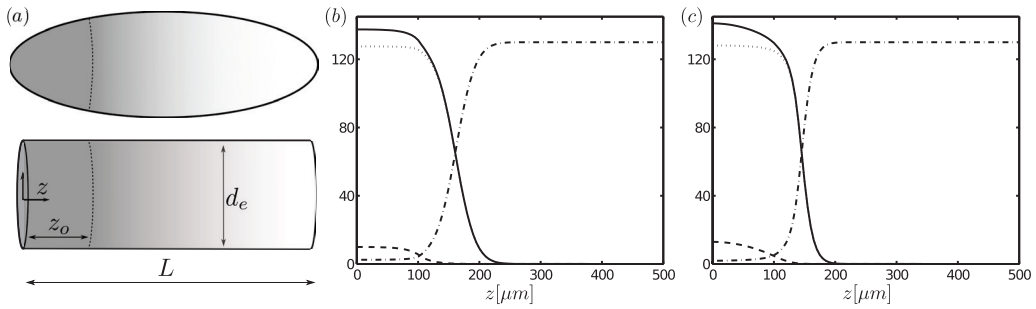


**Figure 1.** (a) Schematic representation of the embryo that is used in the simulations. The integration domain is a cylinder of length, $L$, and diameter $d_e$. No distinction is made between cytoplasm and nuclei. The coordinate, $z$, runs along the direction along the antero-posterior axis. In the model, Bcd is assumed to be synthesized uniformly over the region $z < z_o$. The gray shade represents the Bcd gradient that is eventually obtained with the simulations. (b)–(c) Numerically simulated concentration distributions at $t = 100$ min and along the AP axis of $\mathrm{Bcd}_T$ (solid curve), *Bcd* (dashed curve), $\mathrm{Bcd}_b$ (dotted curve) and $S$ (dashed–dotted curve). All concentrations are in nM. (b) Results of the model with partial degradation, $\tilde{\alpha} = 0.05\,\mathrm{s}^{-1}$ and $\theta_0 = 0.5\,\mathrm{nM\,s}^{-1}$. (c) Results of the model with total degradation, $\overline{\alpha} = 0.0005\,\mathrm{s}^{-1}$ and $\overline{\theta}_0 = 0.1\,\mathrm{nM\,s}^{-1}$.

generically refers to the protein. In this model we assume that all Bcd, free or bound to sites, is fluorescent.

### 2.2. Analytical estimations: the SDID model under the fast reactions approximation

The SDID model in all of its versions is a reaction–diffusion system. The analysis of this kind of systems may be complicated. Hereby, in order to interpret some results and choose *a priori* some parameters we introduce an approximation where the Bcd transport is described in terms of an effective diffusion coefficient. If we consider that reactions take place on a much faster time scale than diffusion a fast reaction (Strier and Dawson 2000) or *fast buffering* approximation (Wagner and Keizer 1994) can be used. Under this condition the systems given by (11) (or (A.1)) can be described as:

$$\frac{\partial\,[\mathrm{Bcd}]}{\partial t} = D_{\mathrm{coll}}\nabla^2[\mathrm{Bcd}] - \beta D_S|\nabla[\mathrm{Bcd}]|^2 - \hat{\alpha}[\mathrm{Bcd}] + \hat{\theta}(z,t), \tag{12}$$

$$[\mathrm{Bcd}_b] = \frac{[\mathrm{Bcd}][S_T]}{[\mathrm{Bcd}] + K_D}, \tag{13}$$

where $D_{\mathrm{coll}}$ is the effective (collective) diffusion coefficient defined in (8), $\hat{\theta} = \frac{\theta}{1+\frac{[S]^2}{K_d[S_T]}}$, $\beta = \frac{2[S]^3}{K_d^2[S_T]^2(1+\frac{[S]^2}{K_d[S_T]})}$ and $\hat{\alpha} = \frac{\tilde{\alpha}}{1+\frac{[S]^2}{K_d[S_T]}}$, for the partial degradation model (11).

Given that $D_S \ll D_f$, for simplicity we will consider $D_S = 0$. In such a case the term $\propto|\nabla[\mathrm{Bcd}]|^2$ in (12) can be neglected and the first of the equations reduces to:

$$\frac{\partial\,[\mathrm{Bcd}]}{\partial t} = D_{\mathrm{coll}}\nabla^2[\mathrm{Bcd}] - \hat{\alpha}[\mathrm{Bcd}] + \hat{\theta}(z). \tag{14}$$

Although this looks like a linear diffusion equation it is not, since $D_{\mathrm{coll}}$, $\hat{\alpha}$ and $\hat{\theta}$ depend on [Bcd], i.e. they are position and time dependent. The steady-state solution of (14) coincides with that of (11) for $D_S = 0$.

### 2.3. Numerical simulations

We solve the system of equations (11), (A.1) and (A.4) using the Douglas-Ratchford ADI method (Douglas and Rachford 1956). The integration domain is a cylinder of length $L = 500$ $\mu$m with no flux boundary conditions at both ends. We list in table 1 the parameter values that we use. For the concentrations, dissociation constant and free diffusion coefficients we use the estimates presented in Sigaut *et al* (2014) which were derived from an analysis of the experiments of Abu-Arish *et al* (2010). We show in section 3.1 how the rest of the parameters were chosen.

**Table 1.** Common simulation parameters to all SDID model versions. The rates of Bcd degradation and synthesis and of GFP maturation used in the different versions are given in the text.

| | |
|---|---|
| $D_S$ | 0.095 $\mu\mathrm{m}^2\,\mathrm{s}^{-1}$ |
| $D_f$ | 19 $\mu\mathrm{m}^2\,\mathrm{s}^{-1}$ |
| $k_{\mathrm{off}}$ | 0.1 $\mathrm{s}^{-1}$ |
| $K_D$ | 0.192 nM |
| $[S_T]$ | 130 nM |
| $L$ | 500 $\mu$m |

### 2.4. Choice of parameter values

We here describe how we choose the parameter values in the case of the SDID model with partial degradation. To have a good starting point, we first look at the stationary solution of (11) with the goal of comparing semi-quantitatively the observed fluorescence profile with the (stationary) distribution of the total Bcd concentration, i.e. of $[\mathrm{Bcd}_T] = [\mathrm{Bcd}_b] + [\mathrm{Bcd}]$. To this end we set $D_S = 0$, a reasonable approximation given that $D_S \ll D_f$. Under this approximation, the continuous production of Bcd eventually saturates the binding sites inside the region where Bcd is synthesized (i.e. for $z \leqslant 0.2L$) we estimate that there is a subregion, $z \leqslant 0.2L$ , where [Bcd] and $[\mathrm{Bcd}_T]$ are approximately uniform with *Bcd* and $S$ in equilibrium between themselves:

$$[\mathrm{Bcd}_b] = [\mathrm{Bcd}][S_T]/([\mathrm{Bcd}] + K_d), \tag{15}$$

$$[S] = K_d[S_T]/([\mathrm{Bcd}] + K_d), \tag{16}$$

and where there is a balance between the rate of Bcd production and degradation. Thus, we expect the stationary solution to satisfy:

$$[\mathrm{Bcd}] \approx \frac{\theta}{\tilde{\alpha}}, \tag{17}$$

$$[\mathrm{Bcd}_b] \approx \frac{\theta}{\tilde{\alpha}} \frac{[S_T]}{\theta/\tilde{\alpha} + K_d}, \tag{18}$$

close to the anterior pole. The observed Bcd concentration has been estimated as ∼140 nM at the anterior pole (Abu-Arish *et al* 2010). Therefore, we choose $\theta/\tilde{\alpha}$, so that $[\mathrm{Bcd}_T] = [\mathrm{Bcd}_b] + [\mathrm{Bcd}] \approx 140\,\mathrm{nm}$ at $z = 0$.

Outside the region of Bcd synthesis ($0.2L \leqslant z \leqslant L$), the stationary solution also satisfies the equilibrium condition (15) and (16). The stationary distribution of free Bcd, $[\mathrm{Bcd}]_s$, in this region then satisfies:

$$0 = D_f \nabla^2 [\mathrm{Bcd}]_s - \tilde{\alpha} [\mathrm{Bcd}]_s. \tag{19}$$

Thus, it is given by equation (4) with $z_o$ equal to:

$$z_{o_f} \equiv \sqrt{D_f/\tilde{\alpha}}\,. \tag{20}$$

$[\mathrm{Bcd}_T] = [\mathrm{Bcd}_b] + [\mathrm{Bcd}]$ decays with a different lengthscale. Namely, defining $z_{o_T} \equiv [\mathrm{Bcd}_T]/|\nabla[\mathrm{Bcd}_T]|$ (for $z > 0.2L$) and using (4) and (15) we obtain

$$\frac{z_{o_f}}{z_{o_T}} = \frac{D_{\mathrm{sm}}}{D_{\mathrm{coll}}}, \tag{21}$$

where $D_{\mathrm{sm}}$ and $D_{\mathrm{coll}}$ are given by (7) and (8) with $D_S = 0$. Clearly, (21) does not prescribe a single lengthscale, $z_{o_T}$, since $D_{\mathrm{sm}}$ and $D_{\mathrm{coll}}$ depend on [Bcd] which is not uniform for $z > 0.2L$. However, using some 'typical' concentration values along the gradient we find a first estimate of $\tilde{\alpha}$. In particular, considering that $z_{o_T}$ corresponds to the observed characteristic lengthscale of the fluorescence gradient, $\ell_o \approx (100\text{–}150)\ \mu$m, that $D_f \sim 20\ \mu\mathrm{m}^2\,\mathrm{s}^{-1}$ and that $D_{\mathrm{sm}}/D_{\mathrm{coll}} \approx 0.1$ in the region where FCS experiments are performed (Sigaut *et al* 2014), (20) and (21) yield $\tilde{\alpha} \sim (0.1 - 0.2)\,\mathrm{s}^{-1}$. Then, through the constraint that the total concentration observed at the anterior pole imposes on $\theta/\tilde{\alpha}$ (18), we derive $\theta$. Based on these *a priori* estimates we then explore the parameter space and choose final values that are able to reproduce semi-quantitatively the experimental observations. In particular, we found that $\tilde{\alpha} = 0.05\,\mathrm{s}^{-1}$ allowed to reproduce most properties of the observed gradient. Using this value of $\tilde{\alpha}$, (16) and $[\mathrm{Bcd}_T](z = 0) = 140\,\mathrm{nM}$, we estimated $\theta_0 = 0.5\,\mathrm{nM\,s}^{-1}$.

## 3. Results and discussion

### 3.1. Reproduction of the gradient

Here we show the results obtained through numerical simulations of the SDID model in its different versions and describe how the solutions depend on the various parameters. In the simulations we use the values, $[S_T]$, $D_f$, $D_S$ and $K_d$ derived in Sigaut *et al* (2010). In doing so we are assuming that the free coefficients, $D_f$ and $D_S$, and the total concentration of binding sites are uniform throughout the embryo. For $[\mathrm{Bcd}_T]$ (which we assume changes along the embryo) we only fix its value at the anterior pole based on the results of Sigaut *et al* (2010). We use $L = 500\ \mu$m (Gregor *et al* 2007b) and the rate, $\gamma$, at which Bcd-GFP matures and becomes fluorescent estimated in Drocco *et al* (2011), Liu *et al* (2013). The other parameters are chosen so that the solutions reproduce *semi-quantitatively* the experimental observations of Gregor *et al* (2007b), Little *et al* (2011) as explained in Methods and the appendix.

We show in figure 1(a) a scheme of the simulation domain as explained in Methods and in figures 1(b) and (c) the concentration of the different species along the AP axis obtained at time, $t = 100$ min, using the partial (b) and total degradation models (c) with the parameters of table 1 and the others as described in the caption. For both models we see that the $\mathrm{Bcd}_T$ profile is consistent with the experimental observations. In particular, its concentration decays to ∼50% of its maximum value at $z = 150\ \mu$m. We also observe that most Bcd molecules are bound at the anterior pole (as estimated in Sigaut *et al* (2014)). As we move away from the anterior pole, $[\mathrm{Bcd}_T]$ begins to decrease and the number of free binding sites increase. Since the mobility of the bound molecules is slower than that of the free ones, the gradient of $[\mathrm{Bcd}_b]$, and hence of $[\mathrm{Bcd}_T]$, is more extended than that of [Bcd]. Comparing figures 1(b) and (c) we observe that the $\mathrm{Bcd}_T$ distribution is slightly different due to the difference in how the Bcd degradation is treated. In particular, near the anterior pole the slope of $[\mathrm{Bcd}_T]$ is more pronounced in the total degradation case. The differences in the length scales obtained with both models is ∼18%. In the case of the model with partial degradation, $[\mathrm{Bcd}_T]$ decays to 10% of its maximum at $z \sim 195\ \mu$m, while in the case with total degradation this occurs at $z \sim 165\ \mu$m. Although this difference might seem significant, it is within the variability found in experiments. On the other hand, as already mentioned, both versions of our model involve a series of simplifications so that we can only expect to obtain a *semi-quantitative* description of the experimental observations, not a complete quantitative agreement. In choosing the parameter values, on the other hand, we preferred to reproduce the distance from the anterior pole at which the concentration decays to a certain percent of its maximum rather than fitting exactly the lengthscale. As we discussed later, assuming a more realistic spatial distribution of the source gives a Bcd distribution that resembles the experimental observations more closely. Figure 1 also shows that in neither model the free or the total Bcd concentrations follow the mRNA distribution given by $\theta(z)$. This implies that, for our model, the Bcd concentration distribution is not a passive reflection of the mRNA that produces it, as assumed in Spirov *et al* (2009).

Comparing the values of $\tilde{\alpha}$ and $\overline{\alpha}$ used in figure 1 with previously reported ones, $0.0003\,\mathrm{s}^{-1}$–$0.0015\,\mathrm{s}^{-1}$ (Gregor *et al* 2007b, Grimm *et al* 2010, Drocco *et al* 2011),

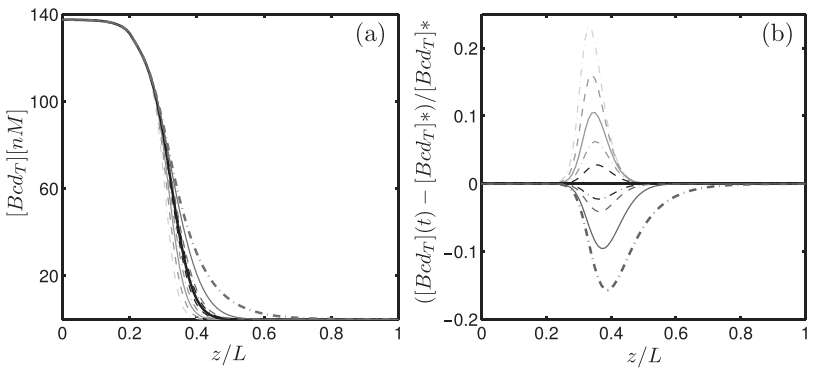


**Figure 2.** (a) Distribution of total Bcd along the AP axis obtained at, increasing from left to right, $t = 50, 60, 70, 80, 90, 100, 110, 120, 167, 833$ min, using the model with partial degradation and the parameters of figure 1(b). The solid curve at the center corresponds to $t = 100$ min, the time at which the gradient is supposedly already established. (b) Differences between $[\text{Bcd}_T]$ at different times and $[\text{Bcd}_T]* \equiv [\text{Bcd}_T](t = 100\ \text{min})$. For $t \in (70, 167)$ min, $[\text{Bcd}_T]$ remains almost constant along the AP axis, except for a small region where the differences are less than 10%.

we observe that the one used in the total degradation model is within this previous estimated range, while the one used in the partial degradation model is larger. This discrepancy is reasonable if we take into account that degradation rates were estimated from fluorescence records that did not distinguish between bound and free Bcd. Namely, if only free Bcd is degraded with rate $\tilde{\alpha}$, (i.e. $\partial[\text{Bcd}]/\partial t \sim -\alpha[\text{Bcd}]$), the rate at which $[\text{Bcd}_T]$ decreases due to degradation is given by $\tilde{\alpha}[\text{Bcd}]/[\text{Bcd}]_T$ (i.e. $\partial[\text{Bcd}_T]/\partial t \sim -\alpha[\text{Bcd}]/[\text{Bcd}]_T\ [\text{Bcd}]_T$). Degradation rates determined from fluorescence images would then correspond to $\tilde{\alpha}[\text{Bcd}]/[\text{Bcd}]_T$. For the parameter values of figure 1(b), this fraction it is $[\text{Bcd}]/[\text{Bcd}]_T \approx \sim 0.08$, which allows to explain in part the discrepancy between the degradation rate used, $\tilde{\alpha} = 0.05\,\text{s}^{-1}$, and the values reported previously in the literature (Gregor *et al* 2007b, Grimm *et al* 2010, Drocco *et al* 2011).

Regarding the rate of protein synthesis, $\theta$, the number of mRNA molecules inside the embryo during n.c. 10–13 was estimated as $\sim 10^5$ molecules (Little *et al* 2011). Considering that mRNA molecules are mainly synthesized over a region that occupies ∼20% of the total length of the embyro, that each molecule can synthesize one protein per second (Milo and Phillips 2015), that the region where nuclei are located and Bcd diffuses is the 20 $\mu$m-wide outermost 'slice' of the embryo and approximating the latter by an ellipsoid of radii ∼250 $\mu$m, 75 $\mu$m and 75 $\mu$m, the $10^5$ mRNA molecules imply a ∼0.3 nM $\text{s}^{-1}$ Bcd synthesis rate. This value is similar to the ones used in the SDID model with partial or total degradation (see figure 1).

So far we have discussed the spatial properties of the gradient. The time it takes for the gradient to be formed is another important aspect that has been debated at large, mainly because the diffusion coefficient estimated in Gregor *et al* (2007b) was too small to account for the gradient formation within the experimentally observed times. Changing the reaction rate, $k_{\text{off}}$, while keeping $K_D$ constant it is possible to modify the timescale over which the reactions take place. We thus explored the predictions of the SDID model using the parameters of figure 1 varying $k_{\text{off}}$ over the range $(10^{-5}$–$10^3)\ \text{s}^{-1}$. We found that the results were mostly insensitive to variations in $k_{\text{off}}$ (data not shown). We observed that the concentration distributions only changed for the most extreme (unrealistic) values of $k_{\text{off}}$. We thus chose $k_{\text{off}} = 0.1\,\text{s}^{-1}$, which we think is reasonable for the type of interactions that Bcd may experience (Milo and Phillips 2015). We show in figure 2(a) the distribution of the total Bcd concentration at various times obtained using the partial degradation SDID model. There we can observe how $[\text{Bcd}]_T$ converges to its asymptotic value with increasing time. In particular, the time it takes for it to be within 5% of the stationary solution is more than $t = 800$ min (≈13 h). This time is much larger than the 100 min observed in experiments (Gregor *et al* 2007b). However, for $t \in (70, 167)$ min the distribution does not change significantly, as illustrated in figure 2(b). During this time interval $[\text{Bcd}_T]$ differs by less than 10% with respect to the concentration at $t = 100$ min and the largest differences are restricted to a very small spatial region. Moreover, the difference with respect to the stationary distribution for $t \geqslant 70$ min is never larger than ∼15% regardless of position. 15% differences are in the border of experimental detectability (particularly, far away from the anterior pole). Our results then suggest, in accordance with the work of Bergmann *et al* (2007), that the steady-state is not reached in less than 100 min but that yet the gradient may seem stationary. In the case of the SDID model with total degradation we observe a similar evolution of $[\text{Bcd}_T]$. For $t \in (80, 120)$ min, $[\text{Bcd}_T]$ varies by less than 20%. Although the rates of production and degradation for the partial and total degradation models are different, the spatio-temporal dynamics of the free and total Bcd concentrations are similar. For this reason, from now on we will present results corresponding to the partial degradation model only.

There is still one property of our simulations that is incompatible with the observations: the maximum concentration ($[\text{Bcd}_T](z = 0)$) is reached almost

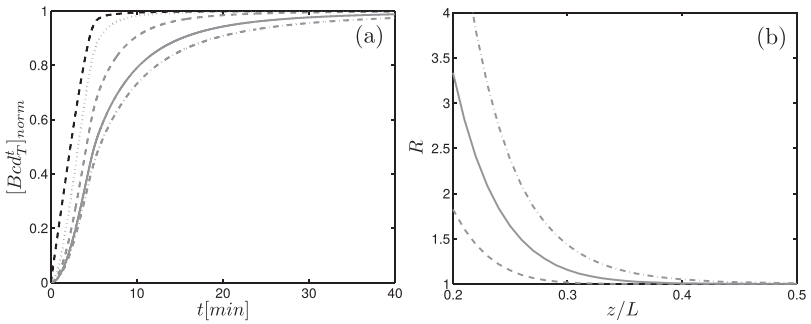


**Figure 3.** (a) Time dependence of the total fluorescent Bcd concentration at the position where the source ends ($z = 20\ \mu$m) obtained through simulations of (A.4) for different rates of GFP maturation (gray dotted line: $\gamma = 0.01\,s^{-1}$, gray dashed line: $\gamma = 0.003\,s^{-1}$, gray solid line: $\gamma = 0.001\,s^{-1}$ and gray dashed–dotted line: $\gamma = 0.0005\,s^{-1}$). The total Bcd concentration obtained without including the process of GFP maturation is shown with a black dashed curve. All parameters are the same as in figure 1(b) and the concentrations displayed are normalized by their corresponding asymptotic values. (b) Ratio of fluorescent to total Bcd, $R$, along the anterior–posterior axis at time, $t = 100$ min for three of the maturation rates probed in (a). Symbols are the same as in (a).

instantaneously. This does not agree with the results of Little *et al* (2011) where it is observed that the maximum is reached 80 min after fertilization. This discrepancy might be due to the finite time it takes for GFP to mature and become fluorescent. To evaluate the effect of maturation we performed numerical simulations of the system given by (A.4). We show in figure 3(a) the total Bcd concentration normalized by its asymptotic value at $z = 100\ \mu$m as a function of time for different maturation rates, $\gamma$. As a reference we also show the corresponding curve for the SDID model with no maturation (black dashed curve). The parameters used in the simulations are the same as in figure 1(b). As expected, the convergence to the asymptotic value takes longer for the model that incorporates maturation and becomes slower as $\gamma$ decreases. For $\gamma = 0.01\,s^{-1}$ we observe little differences between the models with and without maturation. At $t = 10$ min the concentration reaches 98.1% of the asymptotic value in the model with maturation and 99.5% in the model without maturation. In the case with $\gamma = 0.0005\,s^{-1}$ the concentration reached at $t = 10$ min is 73% of the asymptotic value. Hence, for low values of $\gamma$ a significant delay in the convergence is observed in the region close or at the source. The delays obtained, however, never exceeded ∼50% of the time elapsed at very early times and this gap decreased rapidly as time went by. In regions far from the source, the fraction of mature to total Bcd-GFP molecules is larger because it takes longer for the molecules to reach those regions and in that time they mature and become fluorescent. These results are similar regardless of whether we consider the SDID model with partial or total Bcd degradation. This disparity in the delay to reach steady-state depending on the position along the AP axis affects the fluorescence spatial distribution implying a change in the relationship between the lengthscale of the observed gradient and the parameters of the model (Liu *et al* 2013).

To analyze the effect of maturation on the lengthscale we show in figure 3(b) the ratio between total Bcd over fluorescent Bcd, $R(z) \equiv [\mathrm{Bcd}_T]/([\mathrm{Bcd}^f] + [\mathrm{Bcd}_b^f])$. $R$ depends on the relation between $\tilde{\alpha}$ and $\gamma$. In figure 3(b) we show the value, $R$, as a function of $z$ for different values of $\gamma$ ($[0.003–0.001–0.0005]\ s^{-1}$). For all cases $R$ is larger near the source and decreases to ∼1 as the posterior pole is reached. In Liu *et al* (2013) it was determined that $R \sim 3$ close to the source. Of all the considered values of $\gamma$ the one that gives the most similar result to this observation is $\gamma = 0.001\,s^{-1}$. This value of $\gamma$ is in perfect agreement with the rate of degradation of Bcd reported in Drocco *et al* (2011), Gregor *et al* (2007b), Grimm *et al* (2010). The fact that $R$ is a decreasing function of the distance to the source may also affect the lengthscale of the gradient with respect to the case in which GFP maturation is not considered. $R$ decreases very rapidly with distance and at $z = 0.3L$ its value is already very close to 1. For $z > 0.3L$ almost all Bcd molecules are mature and the effect of the immature fraction on the gradient lengthscale can be neglected. In particular, if we compare the distribution, $[\mathrm{Bcd}_T]$, for the same parameters as in figure 3 with and without including the process of GFP maturation the characteristic lengthscales do not show any significant difference.

### 3.2. Interpretation of the experimental observations with a model that includes reactions

The results of the simulations presented so far show that it is possible to reproduce the spatio-temporal characteristics of the Bicoid gradient semi-quantitatively using the SDID model with 'reasonable' biophysical parameter values. We now discuss how the experimentally observed properties are related to the parameters of the model. More specifically, we are interested in determining the relationship between these parameters and the length and timescales of the Bcd gradient and how these relationships change depending on whether the reactions with binding sites are included in the model or not. Thus, we are after a re-interpretation of the observations within the framework of a model that includes reactions. Such a model is nonlinear and the concentrations are not characterized by a single spatial or temporal scale. This becomes evident in the fast reaction approximation, (14), where the transport rate is determined by an

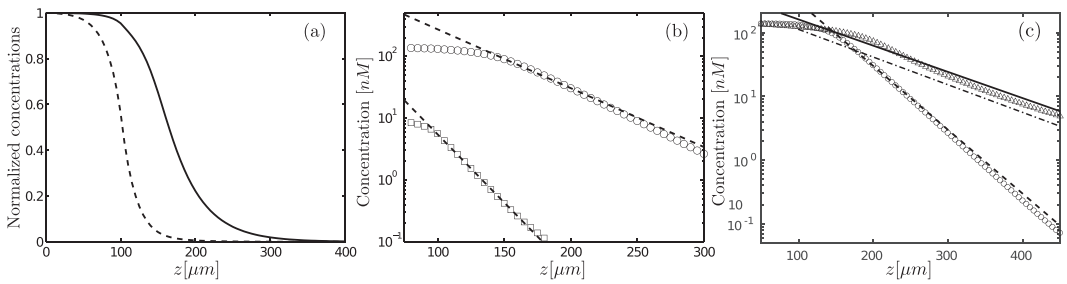


**Figure 4.** (a) Normalized $[\mathrm{Bcd}_T]$ (solid line) and [Bcd] (dashed line) as functions of $z$ at time, $t = 100$ min, obtained from numerical simulations of the SDID model with partial degradation and the same parameters as in figure 1(b). (b) Similar to (a), with the vertical axis on a logarithmic scale ($[\mathrm{Bcd}_T]$ with ○ and [Bcd] with □). The exponential fits to the distributions over the regions $z = (125\text{–}300)\ \mu$m for [Bcd] and $z = (150\text{–}300)\ \mu$m for $[\mathrm{Bcd}_T]$ are superimposed. The characteristic lengthscales obtained with the fits are, respectively, $z_{of} \approx 19\ \mu$m and $z_{oT} \approx 45\mu m$. (c) Similar to (b) for the total Bcd concentration obtained from simulations using the source defined in equation (10) (○) and the source defined in equation (22) which spatial distribution is similar to that of the mRNA determined in Little *et al* (2011) (△). Exponential fits of both curves are superimposed (dashed and solid lines, respectively). The straight line corresponding to the exponential fit of the observed fluorescence obtained in Little *et al* (2011) is also shown (dashed–dotted curve).

effective diffusion coefficient which depends on the concentration, and hence, does not have a single value along the embryo or over time. The presence of 'many' coefficients or 'multiple' scales is in agreement with the work of Little *et al* (2011) in which, in order to reproduce the experimental observations, a model with diffusion coefficients that changed in time *ad hoc* was introduced. This reinforces our idea that it is the effective diffusion coefficients, which naturally arise within the context of the SDID model, that determine the characteristic scales of the problem. Here we seek to relate the effective parameters of the model with the observed spatial scale and the convergence time of the gradient in the simplest possible way. To this end we work with the SDID model with partial degradation and $D_S = 0$. The difference with respect to the SDID model with total degradation is mainly a matter of parameter values. The differences with respect to the model that includes the delay in GFP maturation is discussed later.

### *3.2.1. Lengthscale: free Bcd gradient versus total Bcd gradient*

As discussed in the Introduction, the stationary solution of the SDD model with a source at one end is given by (4) and (5). Within the framework of this model $z_o$ corresponds to the characteristic lengthscale, $\ell_o$, of the observed fluorescence distribution. As described in the methods section, the stationary solution of the SDID model with partial degradation satisfies (13) and (14). Within the context of this model, the lengthscale of the free Bcd concentration, $z_{of}$, is given by (20) (and (A.2) in the case of the SDID model with total degradation). This lengthscale does not correspond to that of the observed gradient because the fluorescence cannot distinguish between free and bound Bcd. Therefore, the observed lengthscale, $\ell_o$, should be related to that of the total Bcd concentration, $z_{oT}$, given by (21). $z_{oT}$ and $z_{of}$ can be very different between themselves. Moreover, $z_{oT}$ changes with position and time.

We now discuss in what regions (21) provides a good estimate of the characteristic lengthscale of the total Bcd distribution. We show in figure 4(a) the normalized free and total Bcd concentrations as functions of $z$ at $t = 100$ min. The free Bcd distribution decays by 50% for $z \approx 100\ \mu$m, while the total Bcd concentration does it at $z \approx 160\ \mu$m. Although the total concentration does not decay exactly exponentially with $z$ as in (4), it can be approximated by such an expression over a certain range of $z$ values. This is shown in figure 4(b) where we plot $[\mathrm{Bcd}_T]$ and [Bcd], normalized by their maximum values, as functions of $z$. The exponential fits (linear on the logarithmic scale of the figure) were done over the regions $z = (125\text{–}300)\ \mu$m for [Bcd] and $z = (150\text{–}300)\ \mu$m for $[\mathrm{Bcd}_T]$ obtaining $z_{of} \approx 19\ \mu$m and $z_{oT} \approx 45\ \mu$m. These values can be compared with those predicted by (20) and (21). In the case of free Bcd, the characteristic lengthscale given by (20) with the simulation parameters is $z_{of} = 19.5\ \mu$m which agrees with the fitted value. In the case of $[\mathrm{Bcd}_T]$ the comparison is more complicated because the lengthscale of (21) depends on $D_{\mathrm{coll}}$ and $D_{\mathrm{sm}}$ which vary with time and space. If we consider the values, $D_{\mathrm{coll}}$ and $D_{\mathrm{sm}}$ at time $t = 100$ min and over the region where the fitting begins, $z = 150\ \mu$m, we obtain $D_{\mathrm{coll}}/D_{\mathrm{sm}} \approx 2$. Inserting those values in (21) we obtain $z_{oT} \approx 40\ \mu$m which is very similar to the one estimated from the fitting. If instead we consider the values at $z = 180\ \mu$m, the ratio of effective coefficients is $D_{\mathrm{coll}}/D_{\mathrm{sm}} \approx 1.2$, leading to an estimate of $z_{oT} \approx 23\ \mu$m which only differs by a factor of 2 with respect to the fitted value. Thus, (20) and (21) provide good estimates of the characteristic lengthscales of the free and total Bcd concentrations if we use the values of the effective coefficients in the region just contiguous to the source (where concentrations start to decrease). We obtain similar results using (A.2) and (A.3) within the framework of the SDID model with total degradation. The characteristic lengthscale of the total Bcd distribution that we obtain with the simulations of figures 4(a) and (b) differs by a factor of ∼2 with respect to that of the experimental observations (Little *et al* 2011). This discrepancy together with the plateau that we obtain in the region of the source both for the free and for the total Bcd

distributions that is apparent in figure 4(a) can be attributed to the simplified space dependence that we have assumed for the source. Namely, if instead of assuming a step-like dependence as in equation (10) we consider that the source spatial distribution is similar to that of the mRNA shown in figure 3(E) of Little *et al* (2011) we obtain that the exponential fits hold over a larger regions and with larger lengthscales. We illustrate this in figure 4(c) where we plot with triangles the concentration, $[\mathrm{Bcd}_T]$, that we obtain simulating the SDID model with partial degradation and the same parameters as in figures 4(a) and (b) but using a source of the form:

$$\theta(z) = 1.125\ \mu\mathrm{M\ s^{-1}} \exp\left(-\frac{1}{2}\left(\log\left(\frac{z}{10.5\ \mu\mathrm{m}}\right)\right)^2\right). \tag{22}$$

The solid curve corresponds to an exponential fit of the profile which prescribes the characteristic lengthscale, $z_{o_T} = 106\,\mu$m, well in accordance with the experiments. We also plot in figure 4(c) the concentration, $[\mathrm{Bcd}_T]$, of figure 4(a) (open circles) with its exponential fit (dashed line) and a straight (dashed–dotted) line with characteristic lengthscale, $\ell = 100\ \mu$m, as observed experimentally in Little *et al* (2011).

### 3.2.2. *Timescale: effective versus free diffusion coefficients*

The solution of the SDD model given by (1)–(2), for long enough $L$, can be approximated as Bergmann *et al* (2007):

$$[\mathrm{Bcd}](z,t) = \frac{\zeta}{A\sqrt{\alpha D}}\left(\exp(-z/z_o) - \frac{\exp(-z/z_o)}{2}\mathrm{erfc}\left(\frac{2Dt/z_o - z}{\sqrt{4Dt}}\right) - \frac{\exp(z/z_o)}{2}\mathrm{erfc}\left(\frac{2Dt/z_o + z}{\sqrt{4Dt}}\right)\right), \tag{23}$$

where erfc is the complementary error function, $\mathrm{erfc}(z) = 1 - \int_0^z \exp(-t^2)\mathrm{d}t/\sqrt{\pi}$. This equation shows that the approach to the stationary solution (4) occurs as if there was a front that travels at speed:

$$v \equiv 2\frac{D}{z_o} = 2\sqrt{\alpha D}, \tag{24}$$

that depends on the diffusion coefficient $D$ and the rate of degradation $\alpha$, and allows to define a convergence time at a distance $z$ from the source as:

$$t_{\mathrm{conv}}(z) \equiv \frac{z}{\sqrt{\alpha D}}. \tag{25}$$

Thus, if $D$ is known *a priori* and $\alpha$ is chosen so that the theoretical characteristic lengthscale of (5) corresponds to the observed fluorescence lengthscale, $\ell_o \sim 100\ \mu$m, the convergence time can be rewritten as:

$$t_{\mathrm{conv}}(z) \equiv \frac{z\ell_o}{D}. \tag{26}$$

At $z = 0.75L$, this time is too long ($\geqslant 10hs$) if it is assumed that $D \approx 1\mu^2\mathrm{m\,s^{-1}}$, the value estimated in Abu-Arish *et al* (2010), Gregor *et al* (2007b) using FRAP, and it is too short ($\sim$0.5 hs) if the free diffusion coefficient of Bcd estimated in Sigaut *et al* (2014), $D \approx 20\,\mu^2\mathrm{m\,s^{-1}}$, is used instead. The solution (23) also shows that the rate of production, $\theta_o$, determines the maximum value of [Bcd] but is not involved in the convergence time.

In the case of the SDID model it is more difficult to define a 'propagation speed' because in addition to the characteristic Bcd degradation time there are other timescales related to the reaction. In order to derive a propagation speed in such a case we then work with the reduced equations in the fast reaction approximation ((14) and (13)). Given the formal equivalence between (14) and (1)–(2) we define the speed and the convergence time as in (24) and (25) but using $D_{\mathrm{coll}}$ instead of $D$ and $\tilde{\alpha}$ instead of $\alpha$. We obtain:

$$v = \sqrt{\tilde{\alpha}\frac{D_{\mathrm{coll}}^2}{D_f}}, \quad t_{\mathrm{conv}}(z) = z\left(\frac{D_f}{\tilde{\alpha}D_{\mathrm{coll}}^2}\right)^{1/2}, \tag{27}$$

for the model with partial degradation and

$$v = \sqrt{\overline{\alpha}\frac{D_{\mathrm{coll}}^2}{D_{\mathrm{sm}}}}, \quad t_{\mathrm{conv}}(z) = z\left(\frac{D_{\mathrm{sm}}}{\overline{\alpha}D_{\mathrm{coll}}^2}\right)^{1/2}, \tag{28}$$

for the model with total degradation. As we did for the lengthscale, we now analyze whether the solution obtained numerically for the model with partial degradation moves with the speed described by (27), if it is possible to define a single characteristic value for the speed in the region immediately adjacent to the source and, in that case, which effective diffusion coefficients determine it. As in the case of the SDD model, if the value, $\tilde{\alpha}$, is determined setting $z_{o_T} = \ell_o$ with $\ell_o$ the observed fluorescence lengthscale and $z_{o_T}$ given by (21)–(20) with known values of $D_f$ qne $D_{\mathrm{sm}}/D_{\mathrm{coll}}$, the convergence time can be rewritten as:

$$t_{\mathrm{conv}} = \frac{D_{\mathrm{sm}}\ell_o z}{D_{\mathrm{coll}}^2}. \tag{29}$$

The same expression is obtained for the model with total degradation using (A.3) and (A.2) and setting $z'_{o_T} = \ell_o$. It then follows that if the degradation rate, $\tilde{\alpha}$ or $\overline{\alpha}$, is derived from the observed fluorescence lengthscale, the convergence time to the steady state solution will be the same regardless of whether we use the model with total or partial degradation. We now continue the analysis for the model with partial degradation.

In order to represent the advancement of the Bcd front and characterize its timescale we compute for each position, $z$, the time, $t$, at which the free Bcd concentration, $[\mathrm{Bcd}(z,t)]$, reaches 50% of its asymptotic maximum value, $\max_t[\mathrm{Bcd}(z,t)]$. We plot in figure 5 the position, $z$, versus the time, $t$, just defined. The slope of this curve corresponds to the propagation speed. As expected in this case the front does not move with a constant speed. It can be observed that the speed is smaller the larger $z$ is. As for the analysis

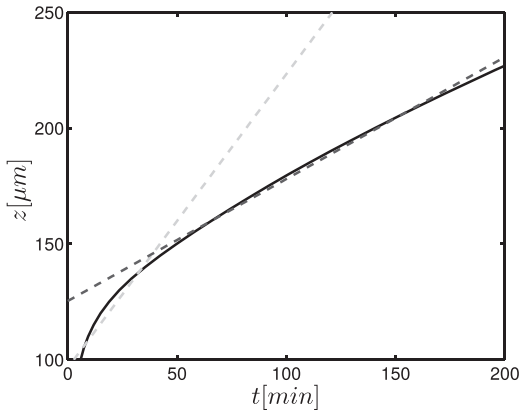


**Figure 5.** Position along the AP axis and time, $(t, z)$, at which the free Bcd concentration reaches 50% of its asymptotic value at the same $z$ in the case of the model with partial degradation (solid line) and the same parameters of figure 1(b). To estimate the rate at which the gradient converges to its steady state two linear fittings were done in different regions along the AP axis (dashed lines).

of the lengthscale, here we focus on a region where the speed is approximately constant. Based on the results of figure 5 we fit the front profile with a linear function in two regions: $z \in [100, 150]$ $\mu$m (light dashed line) and $z \in [150, 225]$ $\mu$m (dark dashed line). From the fits we determine the speeds $v \approx 1.3$ $\mu$m min$^{-1}$ in the region closest to the source and $v \approx 0.53$ $\mu$m min$^{-1}$ in the region further away. This implies that at a distance of the source of the order of the observed fluorescence lengthscale, $z \sim$ (100–140) $\mu$m, the convergence time is of the order of 77–100 min, similar to the characteristic time of the gradient formation obtained experimentally (∼90 min). We must point out that even if we here analyze the convergence of the free Bcd concentration to its steady state solution, the total Bcd (free and bound) reaches its asymptotic distribution on a similar timescale.

We now analyze whether there is a simple expression that can be used to estimate the speed and the convergence time. To this end we compare the speed estimates of figure 5 with those predicted by (27). The latter gives $v(z = 140\ \mu\text{m}, 50\ \text{min}) \approx 1.5$ $\mu$m min$^{-1}$ and $v(z = 180\ \mu\text{m}, 100\ \text{min}) \approx 0.4$ $\mu$m min$^{-1}$. These estimates are similar to those derived with the fitting. We then conclude that it is possible to relate the model parameters with the timescale of the Bcd gradient formation in a relatively simple way. (27) also highlights the importance of distinguishing between the collective and single molecule diffusion coefficients. If in (27) we replace $D_{\text{coll}}$ by $D_{\text{sm}}$ the estimates of the front velocity decrease by approximately one half implying that the timescale would be twice the value derived before.

### *3.2.3. The distinction between free and total Bcd and the role of Bcd as a transcription factor*

As we have already mentioned, Bcd acts as a transcription factor for the expression of hb. This process has been studied in detail both experimentally and theoretically (Gregor *et al* 2007a, Tkačik *et al* 2008, Dubuis *et al* 2013). In particular, the observed (fluorescence) distributions coming from Bcd and Hb in fixed embryos have been used to develop the theory. These distributions were found to be related by a non-linear function with Hill coefficient $n = 5$, i.e. consistent with a high degree of cooperativity of Bcd for the transcription of hb (Gregor *et al* 2007a). These observations, however, cannot distinguish between free and bound Bcd. Here we explore how these observations should be re-interpreted when the interaction of Bcd with binding sites is taken into account. The concentration of the specific hb regulatory sites on DNA is very small compared to the $[S_T]$ value that we have used in the simulations (∼130 nM) which is consistent with the variety of species (Liu and Ma 1996, Rivera-Pomar *et al* 1996, Zhu and Hanes 2000, Guruharsha *et al* 2011) that $S$ represents. Thus, it is reasonable to assume that binding of Bcd to the promoters of the hb transcription does not alter significantly the concentrations of free or bound Bcd that enter the scheme (6). This assumption allows us to readily use the results obtained with the simulations described in the previous sections. Namely, we assume that the concentrations prescribed by our model with $S$ representing non-specific binding sites are not altered significantly by the Bcd binding related to the transcription of hb. We then assume that Hb and (free) Bcd are related by equation (9) with $\overline{K}_D \equiv [\text{Bcd}]_{1/2}$, an effective dissociation constant between Bcd and the sites on DNA that are specific for the transcription of hb. The aim of this section is to analyze to what extent the Hill coefficient that may be derived from the fluorescence distributions provides information on the coefficient, $n$, that enters equation (9) which is somehow related to the cooperativity with which Bcd binds to the hb promoter. Although it is very likely that this binding is cooperative, in this study we place ourselves in the situation that highlights the most our conclusions. Namely, we assume that [Hb] and (free) [Bcd] are related by equation (9) with $n = 1$. We show in figure 6 the (normalized) concentrations of free and total Bcd obtained with the simulations and that of Hb computed as just described as functions of position along the embryo. Once we have the Hb distribution, we derive the apparent Hill coefficient that relates the two observables of the experiment: the fluorescence distributions that we assume are proportional to [Hb] and to the total (not the free) concentration of Bcd and observe that it can be (much) larger than 1. This is illustrated in figures 6(b) and (c).

We show in figure 6(b) the normalized concentration of Hb as a function of the concentrations of free and total Bcd obtained using equation (9) with $[\text{Bcd}]_{1/2} = \overline{K}_D = 0.5$ nM, $n = 1$ and the distributions, [Bcd] and [Bcd$_T$], that correspond to the stationary solution of the SDID model with partial degradation and the parameters of table 1. We note that the relationship between [Hb] and [Bcd] is hyperbolic while the one

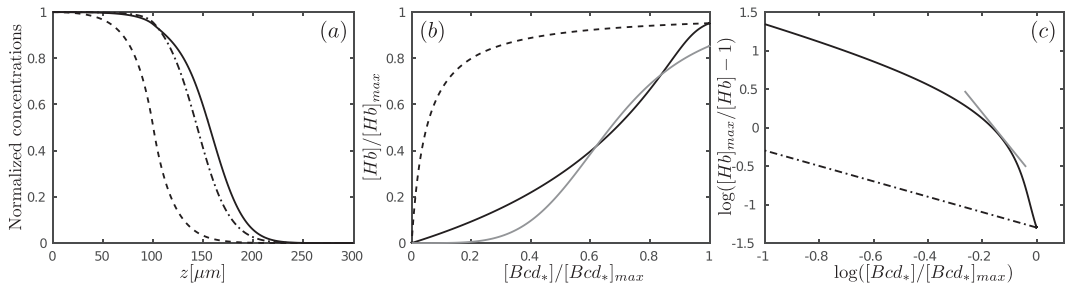


**Figure 6.** (a) Normalized concentrations of total ([$\mathrm{Bcd}_T$], solid curve) and free ([Bcd], dashed curve) Bcd and of Hb (dash-dotted curve), as functions of position along the embryo. (b) Normalized [Hb] as a function of [Bcd] (dashed curve) and of [$\mathrm{Bcd}_T$] (solid curve) and Hill function of the form (30) with $n_f = 4$, [$\mathrm{Bcd}_*$] = [$\mathrm{Bcd}_T$] and [$\mathrm{Bcd}_*$]$_{1/2}$ = 93 nM (gray solid curve). (c) log( [Hb]$_{\max}$ / [Hb] − 1) versus log( [$\mathrm{Bcd}_*$] / [$\mathrm{Bcd}_*$]$_{\max}$) for $\mathrm{Bcd}_* = Bcd$ (dashed curve) and $\mathrm{Bcd}_* = \mathrm{Bcd}_T$ (black solid curve), with the various concentrations computed as in figure 6(a). The gray solid curve has a slope ≈ −4. For all curves, [$\mathrm{Bcd}_T$] and [Bcd] correspond to the solution at $t$ = 100 min of the SDID model with partial degradation and the parameters of table 1 and [Hb] is a function of free Bcd given by equation (9) with $n = 1$ and $\overline{K}_D$ = [Bcd]$_{1/2}$ = 0.5 nM.

between [Hb] and [$\mathrm{Bcd}_T$] is sigmoidal, i.e. characterized by a relationship of the form equation (9) with $n > 1$. The latter ressembles more the experimental observations than the former. In order to analyze how the estimated Hill coefficient may differ from the actual one if it is derived from the fluorescence distributions under the implicit assumption that the Bcd fluorescence is proportional to the free (not the total) Bcd concentration we proceed as follows. We first compute [Hb]/[Hb]$_{\max}$ as in figure 6(a). We assume that this is the relationship that holds in the real system. We then proceed as if we had obtained the distributions of the fluorescence coming from Hb and Bcd in this system and derive an estimated Hill coefficient, $n_f$, from the fit:

$$\frac{[\mathrm{Hb}]}{[\mathrm{Hb}]_{\max}} = \frac{[\mathrm{Bcd}_*]^{n_f}}{[\mathrm{Bcd}_*]^{n_f} + [\mathrm{Bcd}_*]_{1/2}^{n_f}}, \qquad (30)$$

where [Hb] and [$\mathrm{Bcd}_*$] are proportional, respectively, to the Hb and Bcd fluorescence distributions. We compare the estimates of $n_f$ when the fluorescence is proportional to $\mathrm{Bcd}_T$ (i.e. $\mathrm{Bcd}_* = \mathrm{Bcd}_T$) as we think occurs in the real system and when we use $\mathrm{Bcd}_* = Bcd$ instead. To do the fitting we rewrite (30) as:

$$\log\left(\frac{[\mathrm{Hb}]_{\max}}{[\mathrm{Hb}]} - 1\right) = \log\left(\frac{\overline{K}_D^{n_f}}{[\mathrm{Bcd}_*]_{\max}^{n_f}}\right) - n_f \log\left(\frac{[\mathrm{Bcd}_*]}{[\mathrm{Bcd}_*]_{\max}}\right), \qquad (31)$$

where it becomes clear that $n_f$ is the slope of the log( [Hb]$_{\max}$ / [Hb] − 1) versus log( [$\mathrm{Bcd}_*$] / [$\mathrm{Bcd}_*$]$_{\max}$ ) relationship. We show in figure 6(c) log( [Hb]$_{\max}$ / [Hb] − 1) as a function of log( [$\mathrm{Bcd}_*$] / [$\mathrm{Bcd}_*$]$_{\max}$ ) for [$\mathrm{Bcd}_*$] equal to [Bcd] (dashed line) or [$\mathrm{Bcd}_T$] (black solid line). As expected, the relationship is linear in the first case with a slope, $n_f$, that coincides with the actual cooperativity coefficient, $n = 1$. In the other case the relationship is linear for small [$\mathrm{Bcd}_T$] but, as [$\mathrm{Bcd}_T$] increases, the linearity is lost. In particular, the slope changes dramatically in the region where [Hb] is most sensitive to changes in [$\mathrm{Bcd}_T$], [$\mathrm{Bcd}_T$]/[$\mathrm{Bcd}_T$]$_{\max}$ ∼ (0.5−0.8). If the data is fitted using (30) in this region of great sensitivity (see figure 6(c)) we obtain $n_f \approx 4$ which is larger than the actual cooperativity index, $n = 1$. The estimated Hill coefficient, $n_f = 4$, works relatively well when we try to reproduce the [Hb] versus [$\mathrm{Bcd}_T$] relationship as shown in figure 6(b) where we have plotted [Hb]$_{\max}$ / [Hb] computed using equation (30) with [$\mathrm{Bcd}_*$] = [$\mathrm{Bcd}_T$], $n_f = 4$ and [$\mathrm{Bcd}_*$]$_{1/2}$ = 92 nM (gray solid curve). When making this figure we chose the most extreme possible scenario of an underlying coefficient, $n = 1$, and an estimated coefficient, $n_f > 1$. The [Hb] distribution obtained with $n = 1$ is not so similar to the experiments. Using $n = 2$ gives a better [Hb] distribution and an apparent Hill coefficient, $n_f = 7$ (data not shown). In any case, figure 6 serves the purpose of illustrating that the inability to distinguish between free and total Bcd can lead to an overestimation of the Hill coefficient and of the degree of Bcd cooperativity with which hb is transcribed.

Considering that the fraction of Bcd that is involved in Hb transcription is negligible compared to the fraction that is bound to non-specific sites, $S$, could also help understand some of the observations of Liu *et al* (2013) where the spatial location along the embryo where [Hb] decays abruptly was analyzed in embryos with different total amounts of Bcd. As stated in Liu *et al* (2013), 'if Bcd concentration directly controls cell fate [...] the Bcd-dependent patterning markers must always form at the same absolute Bcd concentration'. The results displayed in figure 3 of Liu *et al* (2013) showed that this is the case during early development when the location of the transition point (that is associated to the location of the cephalic furrow) approximately corresponds to a position where the Bcd fluorescence reaches a fixed value. However, later on a dynamic adaptation occurrs so that the point moves towards a fixed position along the embryo, not a fixed fluorescence value. Our model provides a means to reconcile these observations: since [Hb] is a function of free Bcd while the Bcd fluorescence is proportional to [$\mathrm{Bcd}_T$], changing [$S_T$] we could have larger [$\mathrm{Bcd}_T$] values and the same free Bcd concentration. We illustrate this in figure 7 where we compare the

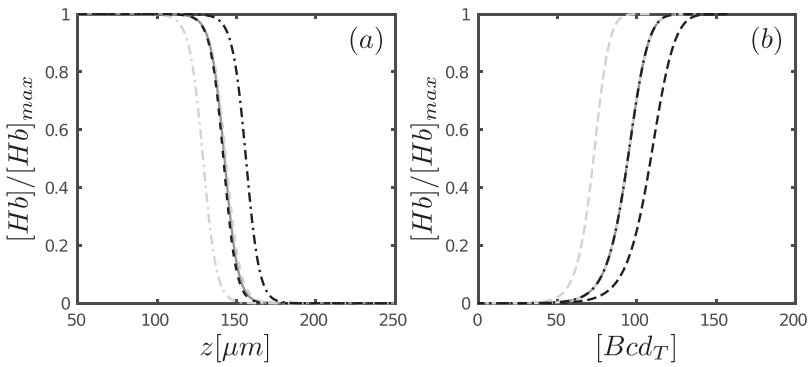


**Figure 7.** Normalized [Hb] as a function of position (a) and of [$Bcd_T$] (b) for the same simulation as in figure 6(a) (gray solid curve) and for similar simulations but with $[S_T] = 150$ nM (gray dashed curve), $[S_T] = 100$ nM (black dashed curve), for a Bcd production rate half (black dashed–dotted curve) or twice as large (grey dashed–dotted curve) as that of figure 6(a). The curves obtained with different $[S_T]$ values are indistinguishable in (a) and those obtained with different source strengths are indistinguishable in (b).

normalized [Hb] distributions that we obtain with the simulation of figure 6(a) and with similar simulations but with different values of $[S_T]$ or of the Bcd source strength as functions of position along the embryo in (a) and of [$Bcd_T$] in (b). There we observe that increasing the rate of Bcd production increases the average [$Bcd_T$] ($\langle[Bcd_T]\rangle = 42.4$ nM for the reference case shown with gray solid curves; $\langle[Bcd_T]\rangle = 37.6$ nM and $\langle[Bcd_T]\rangle = 48.1$ nM for half or twice the Bcd source strength, respectively) and a fixed [Hb]/$[Hb]_{max}$ value corresponds to a fixed [$Bcd_T$] (i.e. fluorescence) value and different positions along the embryo. This is similar to the observations of Liu *et al* (2013) at early times. If we increase $[S_T]$ instead, the average [$Bcd_T$] increases as well ($\langle[Bcd_T]\rangle = 37.6$ nM for $[S_T] = 100$ nM and $\langle[Bcd_T]\rangle = 48.1$ nM for $[S_T] = 150$ nM) but a fixed [Hb]/$[Hb]_{max}$ value corresponds to a fixed position along the embryo and different values of [$Bcd_T$]. Although the real problem is much more complicated than what our model can describe, these results indicate that the dynamic change in the cephalic furrow position with time might be related to an increase of the Bcd 'traps' that the cell may start to produce in the presence of larger Bcd concentrations.

## 4. Conclusions

Understanding the processes that lead to cell differentiation during embryogenesis is a key goal of scientific research (Wolpert 1969, Crick 1970). Advancing in this regard is not only relevant to improve the comprehension of how life and living organisms are shaped but also of the limits that physics imposes on such processes (Tkačik *et al* 2008, Dubuis *et al* 2013). The case of the patterning along the anterior–posterior axis of *Drosophila melanogaster* embryos is an example that has been studied in great detail both experimentally (Driever and Nusslein-Volhard 1989, Gregor *et al* 2007a, 2007b, Little *et al* 2011, 2013) and through modeling (Driever and Nusslein-Volhard 1988, Bergmann *et al* 2007). The gradient of the protein Bicoid (Bcd) which acts as transcription factor for the production of other proteins, is key for this process. The Bcd system, on the other hand, provides a paradigmatic example of the difficulties of quantifying biophysical and biochemical parameters from fluorescence observations. The *SDD* model (Driever and Nusslein-Volhard 1989, 1988) was proposed to explain the formation of the Bcd gradient in *Drosophila melanogaster* embryos but it could not account satisfactorily for all its observed characteristics. In particular, the estimates of the Bcd diffusion coefficient derived in Gregor *et al* (2007b) using FRAP were too small to explain the establishment of a stable gradient within the times observed experimentally. The estimated diffusion rate was challenged by new measurements obtained with FCS (Abu-Arish *et al* 2010, Porcher *et al* 2010). These apparently contradictory results on Bcd diffusion could be explained within a unified model in Sigaut *et al* (2014) by considering that, in the embryo, Bcd not only diffuses freely but also interacts with binding sites, a process that naturally occurs in this case given that Bcd is a transcription factor. According to this unifying model Bcd diffuses with a free coefficient, $D_f \sim 20\ \mu m^2\ s^{-1}$, and a large fraction of it is bound to immobile or very slowly moving ($D_S \sim 0.1\ \mu m^2\ s^{-1}$) sites so that FRAP and FCS experiments provide information on the *effective* coefficients of (7) and (8) (Sigaut *et al* 2010, 2014). In this paper we have studied if this type of *SDID* model with the diffusion coefficients, concentrations and dissociation constant estimated in Sigaut *et al* (2014) can explain the formation of a Bcd gradient with the space and time properties observed experimentally. In spite of its simplicity, the model provides an ideal platform where to analyze how the characteristic length and time scales of [Bcd] are affected when the interaction with binding sites is considered. In order to quantify some unknown parameters we compared the characteristic lengthscale of the observed Bcd gradient with that predicted by the model. Given that Bcd-GFP is fluorescent regardless of whether it is free or bound we interpreted the observed lengthscale as the one that corresponds to the total (not just the free) Bcd

distribution. As discussed in the Methods and Results sections, if Bcd binds to sites the lengthscales of [Bcd] and [Bcd$_T$] differ by a factor $\sim\frac{D_{sm}}{D_{coll}}$ (see (21)) outside the region of Bcd synthesis. This ratio can be arbitrarily small (Pando *et al* 2006) and has been estimated to be ∼0.1 in the anterior end of the embryo during its early stages (Sigaut *et al* 2014). This means that the quantification of biophysical parameters based on the lengthscale of the fluorescence distribution can lead to very different parameter estimates depending on the model with which the observations are interpreted. Since both $D_{sm}$ and $D_{coll}$ are nonlinear functions of the concentrations, their ratio changes with position along the embryo. The simulations of figures 4(a) and (b) estimate it as ∼2 outside the region where Bcd is synthesized. Although this ratio is close to one and does not imply an order of magnitude difference in the parameter estimates that can be derived from the observed lengthscale, according to the simulations of figures 4(a) and (b), [Bcd] and [Bcd$_T$] decay to 50% of their maximum values at very different distances from the anterior end, $z \approx 100$ $\mu$m, and $z \approx 160$ $\mu$m, respectively. This again highlights the implications that a particular choice of model has on the interpretation of the observations. We based our choice of the parameters that were not estimated in Sigaut *et al* (2014) on the fluorescence lengthscale distribution and on the time it takes for the gradient to be established. The quantitative discrepancies between the simulations of figures 4(a) and (b) and the experimental observations (e.g. the lengthscale is ∼45 $\mu$m in the simulations and 100–150 $\mu$m in the experiments (Little *et al* 2011)) can be attributed to the very simple spatial distribution of the source that we used (equation (10)). Repeating the simulations with a source spatial distribution that mimicked that of figure 3(E) of Little *et al* (2011)) we obtained a total Bcd distribution (shown in figure 4(c)) that decayed exponentially over a larger region and with a lengthscale ∼106 $\mu$m, i.e. twice as long as before. In any case, the simulations performed using the simple source (equation (10)) are good enough for the purpose of the present work, which is not to reproduce all the experimental observations with complete quantitative agreement, but to study how the binding/unbinding reactions of Bcd might affect the fluorescence distribution and its interpretation.

The simplicity of the SDD model is very appealing. Within its context, the properties that are observed experimentally are directly related to the parameters of the model. The SDID model is nonlinear and a direct comparison between theory and experiment is more complicated. In spite of this, in this paper we went beyond the numerical simulations and obtained analytical expressions that could describe the simulated results. In this way we could establish that the role that the free diffusion coefficient plays in the SDD model, in the SDID model it is played by the largest of the two effective diffusion coefficients of Pando *et al* (2006) (the collective coefficient of (8)) as illustrated in figure 4 and 5. Had it been the single molecule coefficient that is estimated with FRAP (Sigaut *et al* 2010), the timescale of the gradient formation would have been too large compared to the experimental observations. This is especially important for the action of Bcd as transcription factor and the precision with which its 'bulk' concentration can be estimated by the regulatory binding sites on DNA (Gregor *et al* 2007a, Ipiña and Dawson 2016). Considering the interaction of Bcd with binding sites as done in our SDID model has major consequences for the interpretation of the experiments that seek to quantify the action of Bcd as transcription factor. More specifically, given that the fluorescence does not distinguish between free and bound Bcd, the relationship between the Bcd concentration and that of the proteins, e.g. Hunchback (Hb), whose production it regulates needs to be reassessed. As shown in figure 6 the SDID model predicts that the Hill coefficient that characterizes the relation with Bcd and the production of Hb can be smaller than the one that is directly derived from the scatter plot of the observed fluorescence. This conclusion is derived under the assumption that the fraction of regulatory sites on DNA that Bcd binds to is negligible compared to those that are included in the SDID model which should then correspond to other (non-specific) binding sites. In view of the hopping and sliding model of transcription in which transcription factors bind to non-specific sites for relatively long times (Elf *et al* 2007, Hammar *et al* 2012) and eventually find the specific sites for transcription on the DNA molecule (von Hippel and Berg 1989) and given the fact that Bcd interacts not only with DNA, but also with mRNA and proteins (Liu and Ma 1996, Rivera-Pomar *et al* 1996, Zhu and Hanes 2000, Guruharsha *et al* 2011), it is very likely that this assumption be valid in the case of Bcd. Given that most intracellular messengers are subject to binding/unbinding processes, it is likely that similar problems to those discussed here will be found in other systems. Our results are then not only relevant for the particular case of the Bcd gradient but also have wide implications for the interpretation of fluorescence images in living organisms in general.

## Acknowledgments

This research has been supported by Universidad de Buenos Aires (UBACyT 20020130100480BA), Agencia Nacional de Promoción Científica y Tecnológica (PICT 2013-1301). SPD is a member of Carrera del Investigador Científico (Consejo Nacional de Investigaciones Científicas y Técnicas).

# Appendix

In this appendix we present the versions of the SDID model that we have implemented and analyzed but have not described in detail in the manuscript.

### A.1. The SDID model with total degradation of Bcd

In this case we consider that Bcd is degraded while being free or bound and the dynamic equations read:

$$\begin{aligned}\frac{\partial [\mathrm{Bcd}]}{\partial t} &= D_f\nabla^2[\mathrm{Bcd}] - k_{\mathrm{on}}[\mathrm{Bcd}]([S_T] - [\mathrm{Bcd}_b]) + k_{\mathrm{off}}[\mathrm{Bcd}_b] \\ &\quad -\overline{\alpha}[\mathrm{Bcd}] + \theta(z), \\ \frac{\partial [\mathrm{Bcd}_b]}{\partial t} &= D_S\nabla^2[\mathrm{Bcd}_b] + k_{\mathrm{on}}[\mathrm{Bcd}]([S_T] - [\mathrm{Bcd}_b]) - k_{\mathrm{off}}[\mathrm{Bcd}_b] \\ &\quad -\overline{\alpha}[\mathrm{Bcd}_b], \end{aligned} \tag{A.1}$$

where $\overline{\alpha}$ is the degradation rate. The choice of parameter values is done as in the model with partial degradation. We first derive the stationary solution for $D_S = 0$. In this case the equilibrium condition (15) and (16) does not hold for all $z \geqslant 0.2L$. But if reactions occur on a faster timescale than degradation (as in the 'fast reaction approximation' of (14)), it is possible to assume that (15) and (16) hold approximately at every $z \in [0.2L, L]$. In such a case, the evolution equation for [Bcd] is given by (14) with $\tilde{\alpha} = \overline{\alpha}D_{\mathrm{coll}}/D_{\mathrm{sm}}$ and $\hat{\theta}$ as before. As in the model with partial degradation we estimate the lengthscales of the stationary solution as:

$$z'_{o_f} \approx \sqrt{D_{\mathrm{coll}}/\tilde{\alpha}} = \sqrt{D_{\mathrm{sm}}/\overline{\alpha}}\,, \tag{A.2}$$

for [Bcd], and,

$$z'_{o_T} = z'_{o_f} D_{\mathrm{coll}}/D_{\mathrm{sm}}, \tag{A.3}$$

for $[\mathrm{Bcd}_T]$. Although the ratio between the characteristic lengthscales of [Bcd] and $[\mathrm{Bcd}_T]$ in this case is given by (21) as in the partial degradation model, the lengthscale of the gradient depends on different biophysical parameters. The estimate of the degradation rate, $\overline{\alpha}$, that may be derived from the characteristic lengthscale of $[\mathrm{Bcd}_T]$ in this case is approximately related to the one obtained in the model with partial degradation by $\overline{\alpha} = \tilde{\alpha}D_{\mathrm{sm}}/D_f$. Since $D_{\mathrm{sm}} \ll D_f$, if we use this value of $\overline{\alpha}$ and the model with total Bcd degradation to determine the source intensity as before we obtain a value, $\theta$, that is smaller by a factor, $D_{\mathrm{sm}}/D_f$, with respect to the one derived using the partial degradation model. Taking into account that in the region where FCS experiments are performed $D_{\mathrm{sm}}/D_f \sim 0.05$, using (A.2) and (A.3) we obtain the *a priori* estimate $\overline{\alpha} \sim 0.005\,\mathrm{s}^{-1}$. The numerical simulations performed with this value did not give proper concentration distributions for the different species. Hence we used $\overline{\alpha} = 0.0005\ \mathrm{s}^{-1}$ and $\overline{\theta}_0 = 0.1\mathrm{nM\,s}^{-1}$ instead.

### A.2. The SDID model with with GFP maturation

Experiments use Bcd-GFP to observe the distribution of Bcd. It takes some time for GFP to mature and become fluorescent (Sniegowski *et al* 2005, Iizuka *et al* 2011, Little *et al* 2011). Thus, to interpret the observations it may be necessary to include this process. In such a case we need to distinguish between fluorescent (or *tagged*) and non-fluorescent (or *untagged*) Bcd ($\mathrm{Bcd}^t$ and $\mathrm{Bcd}^u$, respectively) and include the transformation between one another. The equations then read:

$$\begin{aligned}\frac{\partial [\mathrm{Bcd}^u]}{\partial t} &= D_f\nabla^2[\mathrm{Bcd}^u] - k_{\mathrm{on}}[\mathrm{Bcd}^u]([S_T] - [\mathrm{Bcd}^u_b] - [\mathrm{Bcd}^t_b]) \\ &\quad + k_{\mathrm{off}}[\mathrm{Bcd}^u_b] - \tilde{\alpha}[\mathrm{Bcd}^u] - \gamma[\mathrm{Bcd}^u] + \theta(z), \\ \frac{\partial [\mathrm{Bcd}^t]}{\partial t} &= D_f\nabla^2[\mathrm{Bcd}^t] - k_{\mathrm{on}}[\mathrm{Bcd}^t]([S_T] - [\mathrm{Bcd}^u_b] - [\mathrm{Bcd}^t_b]) \\ &\quad + k_{\mathrm{off}}[\mathrm{Bcd}^t_b] - \tilde{\alpha}[\mathrm{Bcd}^t] + \gamma[\mathrm{Bcd}^u], \\ \frac{\partial [\mathrm{Bcd}^u_b]}{\partial t} &= D_S\nabla^2[\mathrm{Bcd}^u_b] + k_{\mathrm{on}}[\mathrm{Bcd}^u]([S_T] - [\mathrm{Bcd}^u_b] - [\mathrm{Bcd}^t_b]) \\ &\quad - k_{\mathrm{off}}[\mathrm{Bcd}^u_b] - \gamma[\mathrm{Bcd}^u_b], \\ \frac{\partial [\mathrm{Bcd}^t_b]}{\partial t} &= D_S\nabla^2[\mathrm{Bcd}^t_b] + k_{\mathrm{on}}[\mathrm{Bcd}^t]([S_T] - [\mathrm{Bcd}^u_b] - [\mathrm{Bcd}^t_b]) \\ &\quad - k_{\mathrm{off}}[\mathrm{Bcd}^t_b] + \gamma[\mathrm{Bcd}^u_b], \end{aligned} \tag{A.4}$$

where $\gamma$ is the rate of GFP maturation. Here we assume that this maturation only affects whether the protein is fluorescent or not but not the properties of its transport, binding or degradation. We also assume that immediately after its synthesis the protein is not fluorescent.

# References


Abu-Arish A, Porcher A, Czerwonka A, Dostatni N and Fradin C 2010 High mobility of bicoid captured by fluorescence correlation spectroscopy: implication for the rapid establishment of its gradient *Biophys. J.* **99** L33–5

Bergmann S, Sandler O, Sberro H, Shnider S, Schejter E, Shilo B Z and Barkai N 2007 Pre-steady-state decoding of the bicoid morphogen gradient *PLoS Biol.* **5** e46

Boon J P, Lutsko J F and Lutsko C 2012 Microscopic approach to nonlinear reaction–diffusion: the case of morphogen gradient formation *Phys. Rev.* E **85** 021126

Crick F 1970 Diffusion in Etibryogenesis *Nature* **225** 421

Douglas J and Rachford H H 1956 On the numerical solution of heat conduction problems in two and three space variables *Trans. Am. Math. Soc.* **82** 421–39

Driever W and Nusslein-Volhard C 1989 The bicoid protein is a positive regulator of hunchback transcription in the early drosophila embryo *Nature* **337** 138–43

Driever W and Nusslein-Volhard C 1988 Stability and nuclear dynamics of the bicoid morphogen gradient *Cell* **54** 83–93

Drocco J A, Grimm O, Tank D W and Wieschaus E 2011 Measurement and perturbation of morphogen lifetime: effects on gradient shape *Biophys. J.* **101** 1807–15

Dubuis J O, Tkačik G, Wieschaus E F, Gregor T and Bialek W 2013 Positional information, in bits *Proc. Natl Acad. Sci.* **110** 16301–8

Elf J, Li G W and Xie X S 2007 Probing transcription factor dynamics at the single-molecule level in a living cell *Science* **316** 1191–4

Estrada J, Wong F, DePace A and Gunawardena J 2016 Information integration and energy expenditure in gene regulation *Cell* **166** 234–44

Gregor T, Tank D W, Wieschaus E F and Bialek W 2007a Probing the limits to positional information *Cell* **130** 153–64

Gregor T, Wieschaus E F, McGregor A P, Bialek W and Tank D W 2007b Stability and nuclear dynamics of the bicoid morphogen gradient *Cell* **130** 141–52

Grimm O, Coppey M and Wieschaus E 2010 Modelling the bicoid gradient *Development* **137** 2253–64

Guruharsha K *et al* 2011 A protein complex network of drosophila melanogaster *Cell* **147** 690–703

Hammar P, Leroy P, Mahmutovic A, Marklund E G, Berg O G and Elf J 2012 The lac repressor displays facilitated diffusion in living cells *Science* **336** 1595–8

Hecht I, Rappel W J and Levine H 2009 Determining the scale of the bicoid morphogen gradient *Proc. Natl Acad. Sci.* **106** 1710–5

Hornung G, Berkowitz B and Barkai N 2005 Morphogen gradient formation in a complex environment: an anomalous diffusion model *Phys. Rev.* E **72** 041916

Houchmandzadeh B, Wieschaus E and Leibler S 2002 Establishment of developmental precision and proportions in the early Drosophila embryo *Nature* **415** 798–802

Iizuka R, Yamagishi-Shirasaki M and Funatsu T 2011 Kinetic study of de novo chromophore maturation of fluorescent proteins *Anal. Biochem.* **414** 173–8

Ipiña E P and Dawson S P 2016 Fluctuations, correlations and the estimation of concentrations inside cells *PLoS One* **11** e0151132

Lecker S H, Goldberg A L and Mitch W E 2006 Protein degradation by the ubiquitin—proteasome pathway in normal and disease states *J. Am. Soc. Nephrol.* **17** 1807–19

Little S C, Tikhonov M and Gregor T 2013 Precise developmental gene expression arises from globally stochastic transcriptional activity *Cell* **154** 789–800

Little S C, Tkačik G, Kneeland T B, Wieschaus E F and Gregor T 2011 The formation of the bicoid morphogen gradient requires protein movement from anteriorly localized mrna *PLoS Biol.* **9** e1000596

Liu F, Morrison A H and Gregor T 2013 Dynamic interpretation of maternal inputs by the drosophila segmentation gene network *Proc. Natl Acad. Sci.* **110** 6724–9

Liu J and Ma J 1996 Fates-shifted is an F-box protein that targets Bicoid for degradation and regulates developmental fate determination in Drosophila embryos *Nat. Cell Biol.* **13** 22–9

Milo R and Phillips R 2015 *Cell Biology by the Numbers* (New York: Garland Science)

Pando B, Dawson S P, Mak D O D and Pearson J E 2006 Messages diffuse faster than messengers *Proc. Natl Acad. Sci. USA* **103** 5338–42

Porcher A, Abu-Arish A, Huart S, Roelens B, Fradin C and Dostatni N 2010 The time to measure positional information: maternal hunchback is required for the synchrony of the bicoid transcriptional response at the onset of zygotic transcription *Development* **137** 2795–804

Rivera-Pomar R, Niessing D, Schmidt-Ott U, Gehring W J and Jackle H 1996 RNA binding and translational suppression by bicoid *Nature* **379** 746–9

Sigaut L, Pearson J E, Colman-Lerner A and Dawson S P 2014 Messages do diffuse faster than messengers: reconciling disparate estimates of the morphogen bicoid diffusion coefficient *PLoS Comput. Biol.* **10** e1003629

Sigaut L, Ponce M L, Colman-Lerner A and Dawson S P 2010 Optical techniques provide information on various effective diffusion coefficients in the presence of traps *Phys. Rev.* E **82** 051912

Sigaut L, Villarruel C, Ponce M L and Dawson S P 2016 Sets of FCS experiments to quantify free diffusion coefficients in reaction–diffusion systems. The case of Ca2+ and its dyes (arXiv:1609.04007)

Sniegowski J A, Phail M E and Wachter R M 2005 Maturation efficiency, trypsin sensitivity, and optical properties of arg96, glu222, and gly67 variants of green fluorescent protein *Biochem. Biophys. Res. Commun.* **332** 657–63

Spirov A, Fahmy K, Schneider M, Frei E, Noll M and Baumgartner S 2009 Formation of the bicoid morphogen gradient: an mRNA gradient dictates the protein gradient *Development* **136** 605–14

Sprague B and McNally J 2005 Frap analysis of binding: proper and fitting *Trends Cell Biol.* **15** 84–91

St Johnston D, Driever W, Berleth T, Richstein S and Nüsslein-Volhard C 1989 Multiple steps in the localization of bicoid RNA to the anterior pole of the Drosophila oocyte *Development* **107 Suppl** 13–9

Strier D E and Dawson S P 2000 Rescaling of diffusion coefficients in two-time scale chemical systems *J. Chem. Phys.* **112** 825–34

Struhl G, Struhl K and Macdonald P M 1989 The gradient morphogen bicoid is a concentration-dependent transcriptional activator *Cell* **57** 1259–73

Tkačik G, Callan C G and Bialek W 2008 Information flow and optimization in transcriptional regulation *Proc. Natl Acad. Sci.* **105** 12265–70

von Hippel P H and Berg O G 1989 Facilitated target location in biological systems *J. Biol. Chem.* **264** 675–8

Wagner J and Keizer J 1994 Effects of rapid buffers on ca2 + diffusion and ca2 + oscillations *Biophys. J.* **67** 447–56

Wolpert L 1969 Positional information and the spatial pattern of cellular differentiation *J. Theor. Biol.* **25** 1–47

Yuste S, Abad E and Lindenberg K 2010 Reaction-subdiffusion model of morphogen gradient formation *Phys. Rev.* E **82** 061123

Zhu W and Hanes S D 2000 Identification of drosophila bicoid-interacting proteins using a custom two-hybrid selection *Gene* **245** 329–39